

The seasonal cycle of polar vortices on terrestrial planets

2 ILAI GUENDELMAN ¹, DARRYN W. WAUGH ², AND YOHAI KASPI ¹

3 ¹*Department of Earth and Planetary Sciences, Weizmann Institute of Science*
4 *234 Herzl st., 76100*
5 *Rehovot, Israel*

6 ²*Department of Earth and Planetary Sciences, Johns Hopkins University*
7 *3400 North Charles Street, 21218*
8 *Baltimore, Maryland*

9 Submitted to PSJ

10 ABSTRACT

11 Polar vortices are common planetary flows that encircle the pole in the middle or high latitudes,
12 and are observed on of the most solar systems' planetary atmospheres. Earth, Mars, and Titan have
13 a polar vortex that is dynamically related to the mean meridional circulation undergoing a significant
14 seasonal cycle; however, the polar vortex characteristics vary between the planets. To understand the
15 mechanisms that influence the polar vortex dynamics, and its dependence on planetary parameters,
16 we use an idealized general circulation model with a seasonal cycle, varying the obliquity, rotation
17 rate, and orbital period. We find that there are distinct regimes for the polar vortex seasonal cycle
18 across the parameter space. Some regimes have similarities to the observed polar vortices, including a
19 weakening of the polar vortex during midwinter at slow rotation rates, similar to Titan's polar vortex.
20 However, other regimes found within the parameter space have no counterpart in the solar system.
21 In addition, we show that for a significant fraction of the parameter space, the potential vorticity
22 latitudinal structure is annular, similar to the observed structure of the polar vortex on Mars and
23 Titan. We also find a suppression of storm activity during midwinter that shares similarities with the
24 suppression observed on Mars and Earth, which occurs in simulations where the jet speed is greater
25 than 60 ms^{-1} . This wide variety of polar vortex dynamical regimes that shares similarities to observed
26 polar vortices suggest that among exoplanets, there can be a wide variability of polar vortices.

27 *Keywords:* Atmospheric circulation(112)–Solar system terrestrial planets(797)–Exoplante atmospheric
28 *variabilitiy(2020)–Planetary climate(2184)*

29 1. INTRODUCTION

30 Polar vortices are a ubiquitous feature of planetary
31 atmospheres, with Earth, Venus, Mars, Titan, Jupiter,
32 Saturn, and possibly Neptune and Pluto all exhibiting
33 polar vortices (e.g., French & Gierasch 1979; Teanby
34 et al. 2008; Dyudina et al. 2008; Luz et al. 2011; Polvani
35 et al. 2010; Mitchell et al. 2015; Adriani et al. 2018).
36 These polar vortices are a fundamental aspect of the
37 atmospheric circulation, and can be the site of unique

38 microphysical and chemical processes, e.g., ozone deple-
39 tion in Earth's stratosphere, CO₂ condensation on Mars,
40 and HCN clouds on Titan. There is no unique defini-
41 tion of a polar vortex, but here we follow Waugh et al.
42 (2017) and define polar vortices as strong, planetary-
43 scale flows that encircle the pole in the middle or high
44 latitudes. The edge of such vortex can be defined by the
45 latitude at which the zonal wind reaches its hemispheric
46 maximum, which is also referred to as the latitude of the
47 atmospheric jet. Alternatively, it can also be defined by
48 a region of high potential vorticity (PV), with the vortex
49 edge being at the latitude with the steepest meridional
50 PV gradients. Here we will use both the terms polar

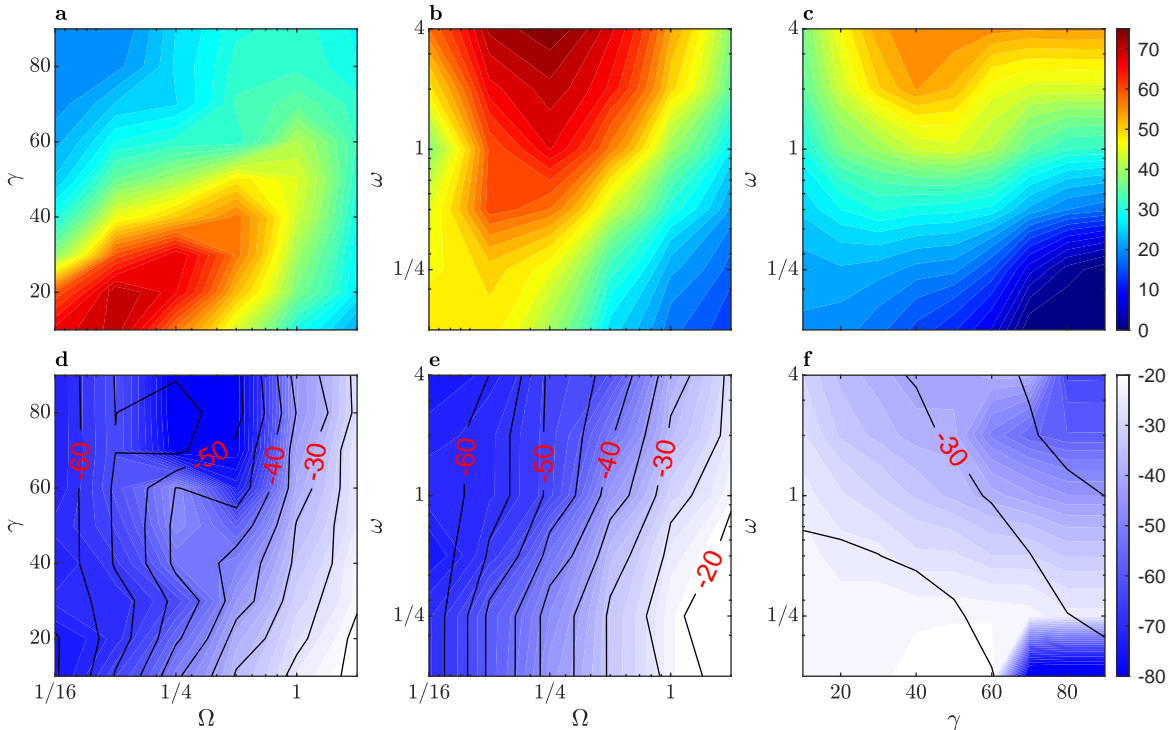


Figure 1. Top row: The maximum wind speed (ms^{-1}), for a vertical mean between $\sigma = 0.25$ and $\sigma = 0.5$ in the southern hemisphere during southern hemisphere winter. Bottom row: The latitude of maximum winds (shading) and latitude of descending branch of the Hadley cell. In a and d, $\omega = 1$, in b and e, $\gamma = 30^\circ$, and in c and f, $\Omega = 1$.

51 vortex and jet, with polar vortex used primarily when
 52 discussing the PV structure and jet when discussing the
 53 zonal wind structure.

54 While polar vortices are common, their characteris-
 55 tics vary among the solar system planets. This includes
 56 not only variations in the size and strength of the polar
 57 vortices, but also their seasonal variability. For exam-
 58 ple, the polar vortices on Earth and Mars are gener-
 59 ally strongest (strongest winds and steepest PV gradi-
 60 ents) around or after the winter solstice (e.g., Mitchell
 61 et al. 2015; Waugh et al. 2017), whereas observations
 62 and model simulations suggest that Titan’s polar vortex
 63 obtains its strongest winds during late fall and the polar
 64 vortex weakens during midwinter (e.g., Lora et al. 2015;
 65 Teanby et al. 2017, 2019). There are also differences in
 66 their PV structure: On Earth, the PV generally has a
 67 monopolar meridional structure with PV maximizing (in
 68 absolute terms) at or near the pole (e.g., Polvani et al.
 69 2010), whereas on Mars and Titan there is an annular
 70 structure with the maximum PV away from the pole
 71 (e.g., Mitchell et al. 2015; Waugh et al. 2016; Sharkey
 72 et al. 2020, 2021). The causes of some differences are
 73 known, but others are not explained and there is a need
 74 to better understand the underlying mechanisms con-
 75 trolling the polar vortex dynamics on the different plan-
 76 ets. This will not only improve understanding of the

77 atmospheric dynamics on these planets, but will also
 78 provide insights into possible structure/evolution of po-
 79 lar vortices on terrestrial exoplanets.

80 Another area where a better understanding is needed
 81 is the relation between polar vortices and storm activity.
 82 In Earth’s troposphere the storm activity over the north
 83 Pacific ocean weakens during midwinter even though
 84 the jet is strongest during this period (Nakamura 1992).
 85 This phenomenon also appears over the north Atlantic
 86 ocean during years with a strong jet (Afargan & Kaspi
 87 2017). The suppression of storm activity during midwin-
 88 ter is in odds with linear models of baroclinic instability,
 89 but can be explained when considering the dephasing of
 90 the baroclinic wave when the jet is stronger (Hadas &
 91 Kaspi 2021). On Mars, similar to Earth, there is also a
 92 suppression of baroclinic activity during solstice, which
 93 is again the period where the jet is strongest (e.g., Lewis
 94 et al. 2016; Mulholland et al. 2016; Lee et al. 2018). Al-
 95 though there are similarities between the two planets,
 96 there are also some differences in the characteristics of
 97 the suppression that occurs on both planets (Lewis et al.
 98 2016). Given that on both planets there is a suppression
 99 of storm activity during the period with the strongest jet
 100 suggests that this suppression can occur in other planets
 101 and there is a need to better understand how common
 102 is this phenomenon in planetary atmospheres.

In this study we seek to understand the dynamics governing these phenomena by varying three planetary parameters, the rotation rate, obliquity, and orbital period, in an idealized three-dimensional general circulation model (GCM). Using this large suite of simulations, we analyze the polar vortex structure, seasonal evolution and its seasonal relation to storm activity. Although the idealized model neglects some processes, such as CO₂ condensation, which was shown to be essential for the polar vortex characteristics on Mars (e.g., [Toigo et al. 2017](#); [Seviour et al. 2017](#)), it simplifies the problem allowing for identification of the key parameters and dynamical processes.

The model used in this study is described in section 2. In section 3 we examine how the jet strength and seasonality depends on the planetary parameters. We show that the flows observed on the solar system terrestrial planets are found within our parameter space and align with the specific planet’s parameters. Additionally, we show new regimes within the parameter space, that do not resemble the flow observed in the solar system terrestrial atmospheres. In section 4 we discuss the relationship between the jet strength and EKE; we show that a midwinter minimum in EKE occurs in our parameter space. Following that, we discuss the PV structure of the polar vortex in section 5, showing that a state of an annular PV, similar to that observed on Mars and Titan, is common. We conclude in section 6.

2. MODEL AND SIMULATIONS

To understand the variability of the polar vortex’s seasonal cycle in planetary atmospheres, we use an idealized GCM with a seasonal cycle based on the GFDL dynamical core ([Guendelman & Kaspi 2019](#)). The model is an aquaplanet GCM with a 10m depth slab ocean. The model is forced at the top of the atmosphere with a diurnal mean seasonal insolation. The radiation transfer in the atmosphere is represented using a two-stream radiation scheme ([Frierson et al. 2006](#)) where we keep the optical depth constant in latitude. The model utilizes a simplified parameterization for moist convection ([Frierson et al. 2006](#)) and neglects different effects such as clouds and ice. Additionally, the simplicity of the model’s radiation scheme and the lack of an ozone layer results in a different flow in the model’s stratosphere compared to that of Earth (e.g., [Tan et al. 2019](#)).

We run simulations varying the rotation rate (Ω) from 1/16 to 2 time Earth’s rotation rate, obliquity (γ) from 10° to 90° and the orbital period (ω) from 1/8 to 4 times Earth’s orbital period, using 360 days in an Earth-like orbital period. We run three different sub-spaces of this parameter space by keeping one of the parameters

constant ($\gamma = 30^\circ$, $\Omega = 1$ and $\omega = 1$) at a T42 resolution and 25 vertical σ levels ($\sigma = p/p_s$, where p_s is the surface pressure). All simulations run for at least 80 Earth years (360 days), and climatology is calculated using the latter 50 years (based on the simulation’s orbital period).

Each of the three parameters has a different effect on the planetary climate. The degree of seasonality is controlled mainly by the planet’s obliquity and orbital period. The obliquity resolves the latitudinal seasonal cycle of the top of the atmosphere solar forcing. The orbital period controls the timescale that the atmosphere has to adjust to radiative changes and plays a crucial role in the resulting seasonal cycle. Unlike the previous two parameters that relate mainly to the atmosphere’s radiative forcing, the rotation rate is a crucial parameter that strongly affects the atmospheric circulation ([Kaspi & Showman 2015](#)).

3. JET STRENGTH AND SEASONALITY

3.1. Parameter space overview

Jets persist across the parameter space explored. In most cases, the strongest jet is in the winter hemisphere. However, for strong seasonality and slow rotation rate there are weak winds in the winter and the prominent vortex is in the summer hemisphere ([Guendelman et al. 2021](#)). In this study, we will mainly focus on the winter jet.

The strength and latitude of the jet varies significantly within the explored parameter space. Figure 1 shows the dependence of the maximum wind speed (top row) and the latitude of the winter jet (bottom row, colors) on the different parameters. The wind speed changes non-monotonically with the rotation rate (Fig. 1a-b), a similar trend was noticed and explained using angular momentum conservation arguments in previous studies ([Kaspi & Showman 2015](#); [Wang et al. 2018](#); [Guendelman et al. 2021](#)). The winds strength dependence on the orbital period is monotonic, where the wind strength increases for longer orbital periods (Fig. 1b-c). The dependence of the maximum wind speed on obliquity depends on the orbital period, for long orbital periods the dependence is non-monotonic with the wind speed maximizing at moderate obliquity values (Fig. 1a,c), which can be explained using considerations of angular momentum conservation ([Guendelman et al. 2021](#)). For short orbital periods, the maximum wind speed decreases monotonically with obliquity (Fig. 1c). This monotonic decrease with obliquity is a result of the dominance of the annual mean climate at short orbital periods. As the obliquity increases, the annual mean insolation meridional gradient decreases and reverses for obliquities larger than 54° ([Guendelman & Kaspi 2019](#)). This in turn results in a

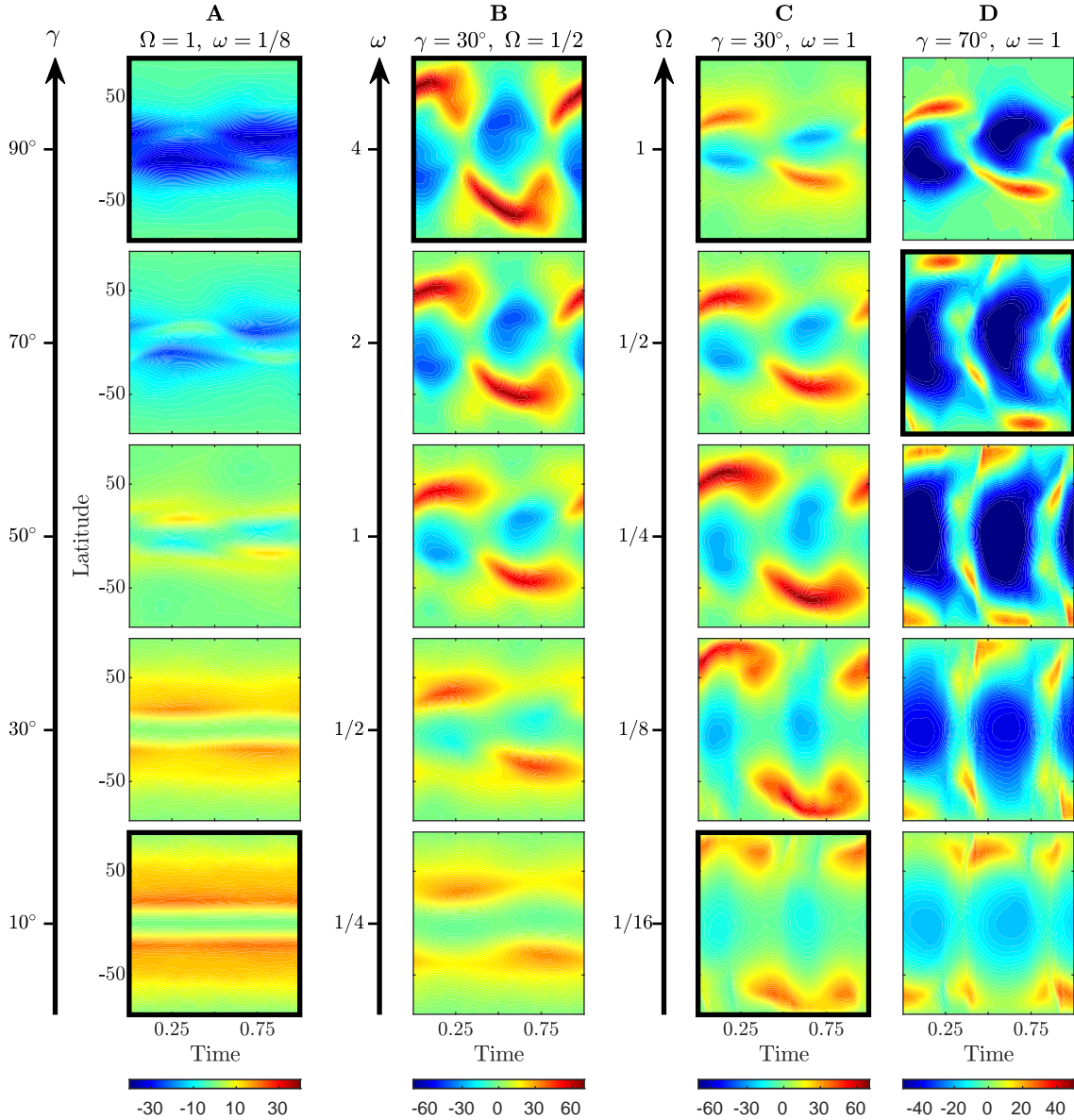


Figure 2. Selected simulations demonstrating the most dominant types of seasonal behavior within the parameter space. Plots shows the zonal mean zonal wind vertically averaged between $\sigma = 0.25$ and $\sigma = 0.5$. Column A shows the jet dependence on obliquity in the case of a short orbital period and Earth-like rotation rate, i.e., weak seasonality. Column B shows the jet dependence on the orbital period for moderate obliquity and rotation rate. Columns C and D show the jet dependence on the rotation rate for Earth-like orbital period, and obliquity 30° and 70° respectively. Highlighted panels are the representative cases of the distinct behavior of the jet in the parameter space and are summarized in Figure 3. Note different colorscale for each column.

205 decrease in the temperature meridional gradient and a
206 weakening of the jet.

207 The variation of the jet's latitude is in good agreement
208 with the latitude of the ascending edge of the Hadley
209 circulation (Fig. 1d-f), indicating that the jet correlates
210 to the mean meridional circulation. That said, there
211 is a misfit for short orbital periods and high obliquity
212 (Fig. 1f), where there are weak westerlies and the max-
213 imum wind speed is close to zero (Fig. 1c), i.e., there is

214 no winter polar vortex. In cases of high obliquities and
215 short orbital periods, the climate has a weak seasonal
216 cycle and reversed temperature gradients (Guendelman
& Kaspi 2019), which results in a significantly different
218 circulation (Kang et al. 2019).

219 In addition to variations in the strength of the winter
220 vortex, the seasonal evolution of the polar vortex de-
221 pends on the planetary parameters (Fig. 2). To show
222 this, we focus our attention on several representative

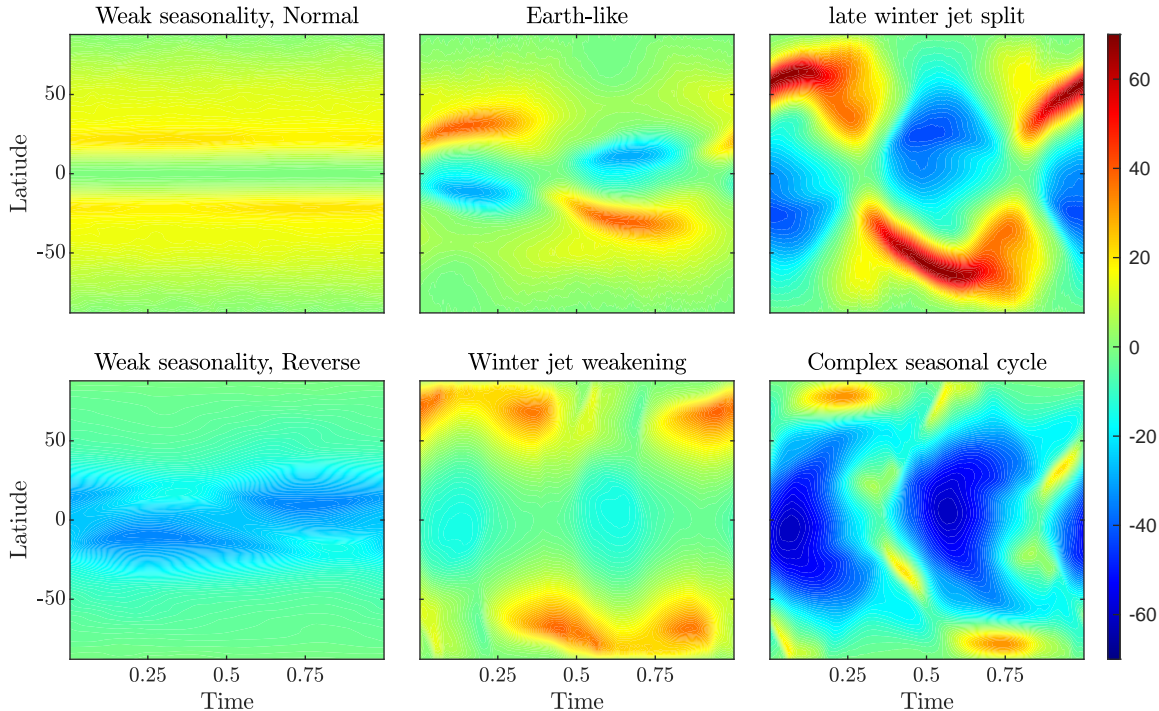


Figure 3. Main distinct regimes of jet (vertical mean wind between $\sigma = 0.25$ and $\sigma = 0.5$) seasonal cycle detected in the parameter space, these panels are the highlighted panels in Figure 2. The details of each case are summarized in the text.

subspaces of our parameter space. First, consider the regime with short orbital periods (Fig. 2A). In this regime, the seasonal variability is weak, and the annual mean climate dominates. At low obliquities, the polar vortex is in the midlatitudes (bottom panel in Fig. 2A); as obliquity increases, the vortex weakens to a point where it no longer exists, and instead of a westerly jet, there is an easterly jet. This is a result of the annual mean insolation gradient dependence on obliquity, where it weakens and reverses as obliquity increases (Guendelman & Kaspi 2019).

Increasing the orbital period increases the seasonal variability and the strength of the jet (Fig. 2B). The jet seasonal cycle becomes more complex as the orbital period is increased, both in terms of its strength and latitudinal position. For cases with intermediate to fast rotation rates with a long enough orbital periods (e.g. $\Omega \geq 1/2$, $\omega > 1/2$ in Fig. 2B), the jet occurs solely between fall and spring, and is strongest and in its most poleward position during midwinter. Additionally, when the orbital period becomes very long the jet splits into two separate jets during late winter (top panel in Fig. 2B).

Consider now the jet variations with the rotation rate (Fig. 2C). In the Earth-like case, i.e., fast rotation rate and moderate obliquity (top panel in Fig. 2C), the dominant jet occurs during winter with only small variations

in its position. Decreasing the rotation rate (going down in Fig. 2), the jet shifts poleward, and its strength varies non-monotonically. At slow rotation rates, the jet develops a unique seasonal cycle where the wind speed weakens during midwinter (bottom panel in Fig. 2C). A similar transition occurs for higher obliquity (Fig. 2D). The jet for intermediate rotation rates with higher obliquity shows a complex seasonal cycle, where the wind speed is non-monotonic during winter, and there is a jet split during late winter (for example, second panel from the top of Fig. 2D). In addition, at high obliquities and slow rotation rates, the summer polar vortex is more dominant than its winter counterpart (Guendelman et al. 2021, bottom panel in Fig. 2D).

Figure 3 shows six specific cases that highlight the different regimes of the jet seasonal cycle detected within the parameter space. The regimes are as follows:

1. Weak seasonality, normal climate - The jet is in the midlatitudes with weak-to-no seasonality. This occurs at low and moderate obliquity and a short orbital period (e.g., $\omega = 1/8$, $\gamma = 10^\circ$ and $\Omega = 1$).
2. Weak seasonality, reverse climate - No polar vortex, easterly winds in the low- and mid-latitudes with weak seasonality. This occurs at high obliquity and a short orbital period (e.g., $\omega = 1/8$, $\gamma = 90^\circ$ and $\Omega = 1$).

- 276 3. Earth-like - The jet strengthens and shifts slightly
 277 poleward during midwinter. This occurs at moder-
 278 ate obliquity and fast rotation rate (e.g., $\omega = 1$,
 279 $\gamma = 30^\circ$ and $\Omega = 1$).
- 280 4. Winter jet weakening - The jet weakens during
 281 midwinter; this is accompanied by a slight pole-
 282 ward shift of the jet. This occurs at moderate-high
 283 obliquity and slow rotation rate (e.g., $\omega = 1/8$,
 284 $\gamma = 10^\circ$ and $\Omega = 1/16$).
- 285 5. Late winter jet split - The jet strengthens and
 286 shifts poleward during winter, and during late win-
 287 ter/spring, the jet splits into two jets. This occurs
 288 at moderate obliquity, moderate-fast rotation rate,
 289 and long orbital period (e.g., $\omega = 1/8$, $\gamma = 10^\circ$ and
 290 $\Omega = 1$).
- 291 6. Double jet with varied seasonality - There exists
 292 subtropical and polar jets, each having a differ-
 293 ent seasonality. This occurs at high obliquity and
 294 moderate rotation rate (e.g., $\omega = 1/8$, $\gamma = 10^\circ$
 295 and $\Omega = 1$).

296 In the remainder of this section, we will examine more
 297 closely the dynamics of these different regimes.

3.2. Weak seasonal cycle

299 First, we consider the regimes with a weak seasonal
 300 cycle, which in our simulations occur for short orbital
 301 periods. The climate and atmospheric circulation on
 302 planets with a short enough orbital period, such that the
 303 annual mean forcing dominate, strongly depends on the
 304 planetary obliquity, which influences the annual mean
 305 insolation.

306 There are two processes that can accelerate and main-
 307 tain a jet. In the first, as a result of an equator-to-
 308 pole temperature differences, a meridional circulation
 309 from warm to cold latitudes develops. Air parcel that
 310 flows from low to high latitudes gains angular momen-
 311 tum, accelerating the jet. A jet that is maintained
 312 through this process is called a thermally-driven jet
 313 (Vallis 2017). The second process that accelerates a jet
 314 occurs in baroclinic unstable regions. Waves that de-
 315 velop in these regions converge momentum towards the
 316 disturbance regions and accelerate an eddy-driven jet
 317 (Vallis 2017). On Earth, these processes occur in prox-
 318 imity, and the resulting jet is called a merged jet; how-
 319 ever, the jet changes its characteristics during the sea-
 320 sonal cycle (Lachmy & Harnik 2014; Yuval et al. 2018).

321 At low obliquities ($\gamma < 54^\circ$), the maximum insolation
 322 and temperature are at the equator, and the circulation
 323 is similar to Earth's annual mean circulation (Fig. 4).
 324 In each hemisphere there is a Hadley cell in the tropics,

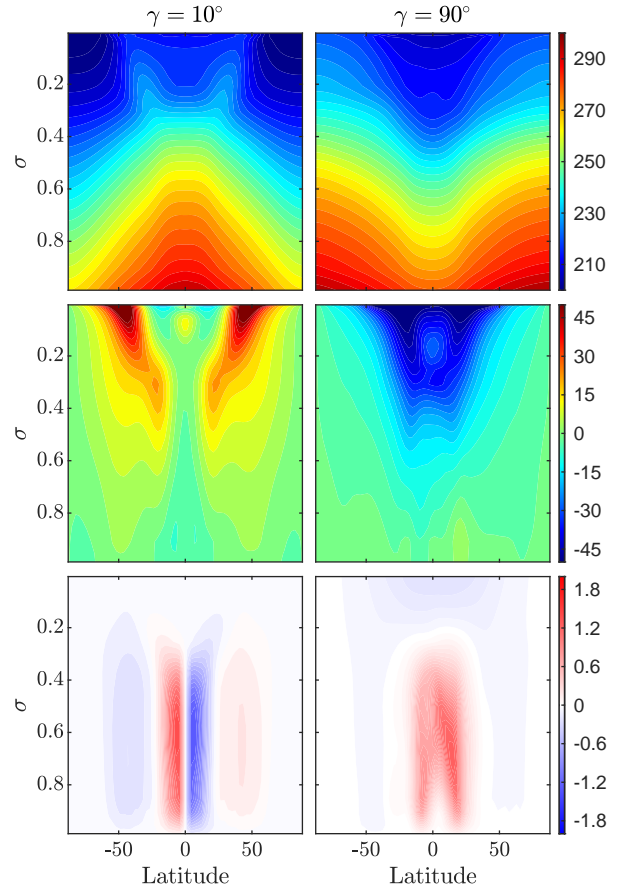


Figure 4. An equivalent June-August temporal mean of the vertical structure of temperature (K, first row), zonal mean zonal wind (ms^{-1} , second row), and mean meridional circulation (Kg s^{-1} , third row, red denotes counter clockwise circulation), for $\gamma = 10^\circ$ (left column) and $\gamma = 90^\circ$ (right column) with $\Omega = 1$ and $\omega = 1/8$.

325 a Ferrel cell in the midlatitudes, and jet between these
 326 two cells (e.g., Vallis 2017). This jet, is a merged jet,
 327 i.e., a merger between the subtropical jet at the edge
 328 of the Hadley circulation and an eddy-driven jet in the
 329 Ferrel cell (e.g., Lachmy & Harnik 2014).

330 In contrast, for high obliquity ($> 54^\circ$) there is a re-
 331 versal of the insolation gradients and the minimum tem-
 332 perature is at the equator. Instead of air ascending at
 333 the equator and descending at the midlatitudes, there is
 334 a cross-equatorial circulation. The warmer hemisphere
 335 dictates the direction of that cross-equatorial circula-
 336 tion, i.e., the cross-equatorial flow will be from the sum-
 337 mer hemisphere (northern hemisphere in Fig. 4) to the
 338 winter hemisphere (summer hemisphere in Fig. 4). This
 339 suggests that, unlike the low obliquity case where small
 340 deviation in the temperature field results in small de-
 341 viations in the circulation, in the high obliquity case,
 342 small changes in the temperature field result in signifi-

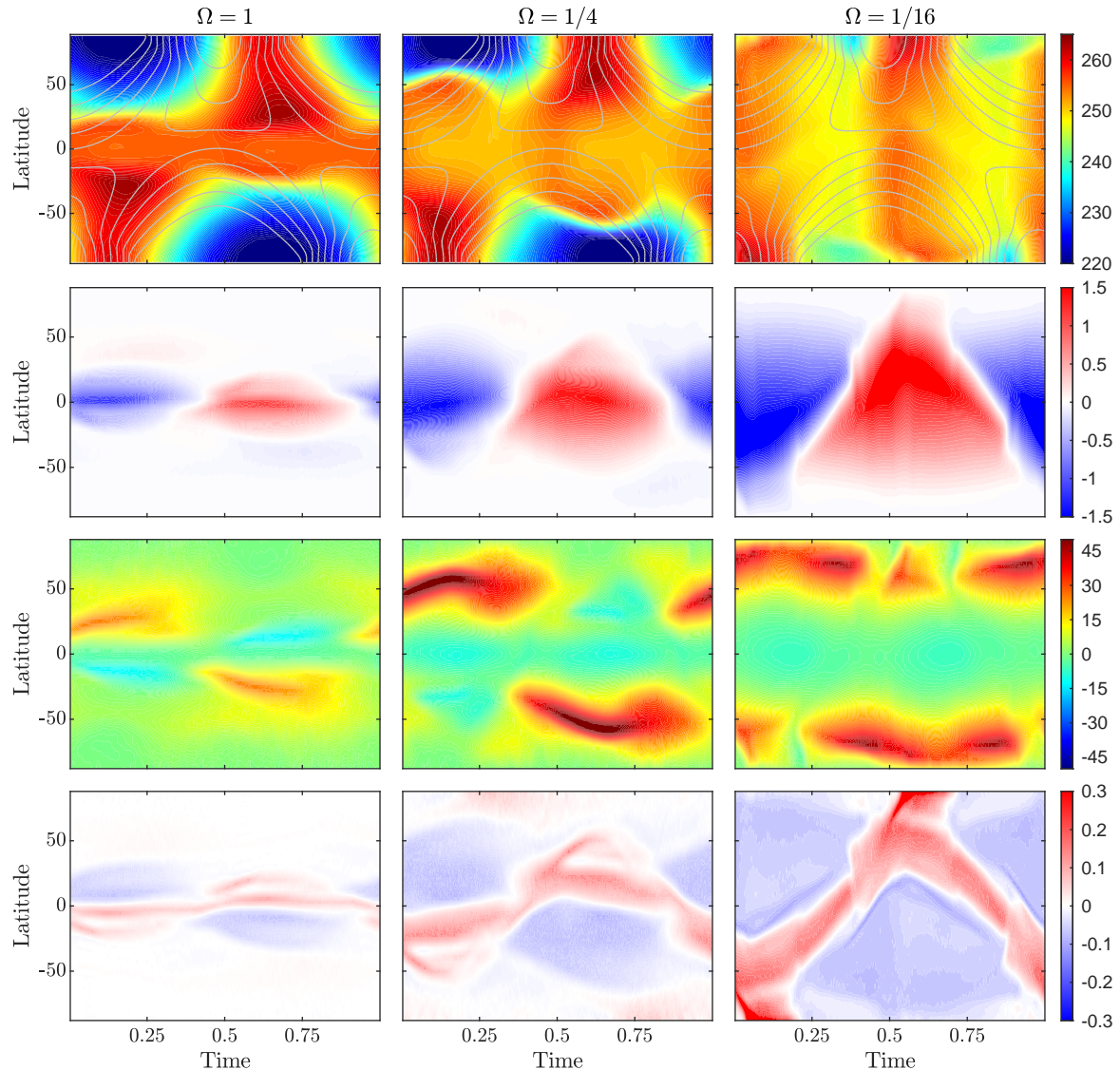


Figure 5. Comparison of the seasonal cycle of three simulations, $\Omega = 1, 1/4$ and $1/16$ with $\omega = 1$, $\gamma = 30^\circ$. Top row: Temperature at $\sigma = 0.5$ (K, shading) and the pattern of the top of the atmosphere forcing (Wm^{-2} , contours). Second row: The mean meridional circulation at $\sigma = 0.5$ (Kg s^{-1} , red is southward flow). Third row: The zonal mean zonal wind at $\sigma = 0.5$ (ms^{-1}). Fourth row: vertical velocity at $\sigma = 0.5$ (Pa s^{-1}).

343 cant variations to the circulation. Furthermore, the annual
 344 mean circulation in the high obliquity case does not
 345 appear during the seasonal cycle, and is an artifact of the
 346 annual averaging. Unlike the meridional circulation, the
 347 zonal mean zonal wind has only small variations during
 348 the seasonal cycle. It consists of weak westerlies close
 349 to the surface, and no westerlies, i.e., no polar vortex at
 350 high altitudes.

351 3.3. Winter jet weakening

352 For Earth-like conditions, the jet strengthens during
 353 the winter, reaching its maximum during midwinter.

354 However, for planets with a slow enough rotation rate
 355 (i.e., $\Omega \leq 0.25$) and a strong enough seasonal cycle (high
 356 obliquity and long orbital period, Figs. 2C-D), the win-
 357 ter jet weakens during midwinter. As the seasonal cycle
 358 becomes stronger, the summer jet weakening occurs at
 359 a faster rotation rate (Figs. 2C-D).

360 To further understand the seasonal transition to a
 361 midwinter weakening of the jet, we compare the sea-
 362 sonal evolution of three cases with different rotation
 363 rates ($\Omega = 1, 1/4, 1/16$) and otherwise the same pa-
 364 rameters ($\omega = 1$ and $\gamma = 30^\circ$). Comparing the latitudi-

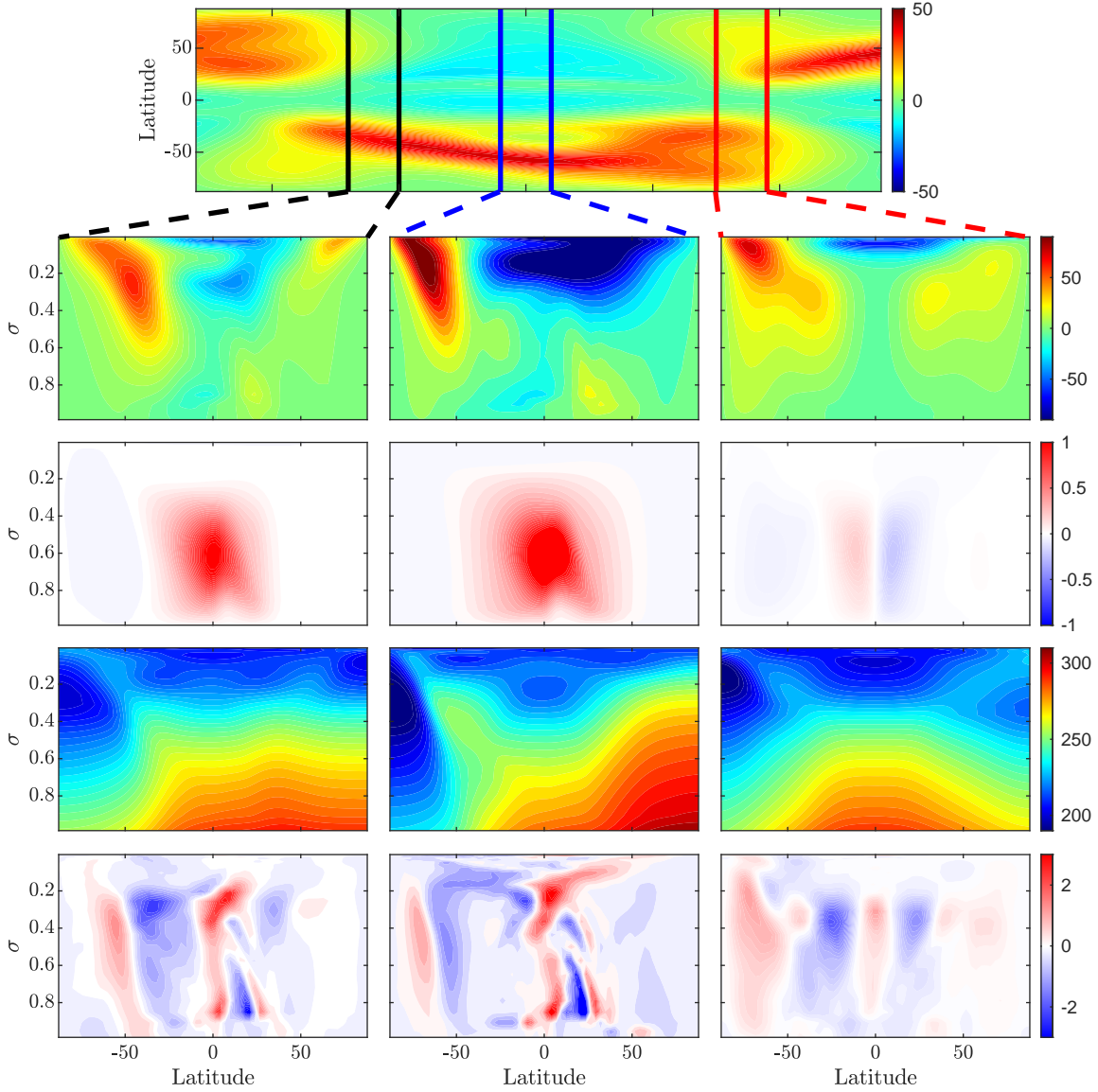


Figure 6. Top row: The zonal mean zonal wind (at a height of $\sigma = 0.5$) around southern hemisphere winter for $\omega = 4$, $\gamma = 30^\circ$ and $\Omega = 0.5$. Vertical lines represent the time average period for the respective columns shown below. Second row: Vertical structure of the zonal mean zonal wind (ms^{-1}). Third row: Vertical structure of the mean meridional circulation ($10^{12} \text{ Kg s}^{-1}$). Fourth row: Vertical structure of temperature (K). Fifth row: Vertical structure of eddy momentum flux convergence ms^{-2} .

365 nal structure of the temperature at $\sigma = 0.5$ and mean
 366 meridional circulation (top two rows in Fig. 5), shows
 367 that regions of weak meridional temperature gradient
 368 correspond to regions with a strong mean meridional
 369 circulation. The weak temperature gradients are the re-
 370 sult of efficient heat transport by the mean meridional
 371 circulation. In addition, the high-level temperature in
 372 the ascending and descending regions of the Hadley cir-
 373 culation are warmer than other latitudes (top row in
 374 Fig. 5). The reason for this warming differs between
 375 the ascending and descending regions. The ascending

376 region is warmer because of the stronger radiative heat-
 377 ing and latent heating occurring in the summer hemi-
 378 sphere, while the descending region is warmer because
 379 of the combined effect of the Hadley cell heat transport
 380 and adiabatic heating due to the descending motion in
 381 this region.

382 The main difference between the regime where the jet
 383 strengthens during midwinter (fast or intermediate rota-
 384 tion rates) and the regime with a midwinter weakening
 385 of the jet (slow rotation rates) is that the Hadley cell
 386 extends from one pole to the other in the latter case,

387 but not the former (third row in Fig. 5). As a result,
 388 in cases with fast and intermediate rotation rates, there
 389 is a strong temperature gradient at high latitudes due
 390 to radiative cooling closer to the pole, as these regions
 391 receive low to no radiation during winter (see insolation
 392 patterns in the top row of Fig. 5). These meridional
 393 temperature gradients maintain the strong jet during
 394 midwinter. However, this is not the case in the slow
 395 rotation rate case, where the temperature gradient is
 396 weak as a result of the expansion of the Hadley circula-
 397 tion and the descending motion being close to the winter
 398 pole (Fig. 5).

399 Examining the seasonal evolution shows that in cases
 400 with fast rotation rates, where the Hadley circulation
 401 width is constrained (e.g., Guendelman & Kaspi 2018),
 402 strong cooling occurs in the winter hemisphere. The
 403 edge of the Hadley cell, which can be inferred from the
 404 temperature field at $\sigma = 0.5$ as a warm patch in the win-
 405 ter hemisphere, is in the jet vicinity. For an Earth-like
 406 rotation rate, where the Hadley cell covers the tropics,
 407 the meridional temperature gradients are not as sharp
 408 as the temperature gradients in the $\Omega = 1/4$ case, where
 409 the descending edge is more poleward. During the sea-
 410 sonal cycle, these gradients become even sharper, and
 411 thus the jet is stronger (Fig. 5). However, in the slow
 412 rotation rate case, the cooling of polar latitudes occurs
 413 only in short periods during spring and autumn, where
 414 descending motion does not reach the poles (bottom row
 415 in Fig 5). In contrast, during winter, the descending mo-
 416 tion is in the polar regions, diminishing the meridional
 417 temperature gradients, resulting in a weaker jet (Fig. 5).

418 To summarize, for slow rotation rates and strong
 419 enough seasonal cycle, the Hadley circulation extends
 420 from one pole to the other during midwinter. The wide
 421 circulation and the descending motion around the pole,
 422 result in weak meridional temperature gradients and a
 423 weak polar vortex during midwinter. This is not the
 424 case for the transition seasons or faster rotation rates.
 425 In these cases, the descending motion is equatorward
 426 of the pole, and the primary process that occurs at the
 427 pole is radiative cooling. The cooling in the polar regions
 428 creates a strong temperature gradient that maintains a
 429 strong polar vortex (Fig. 5).

3.4. Late winter jet split

430
 431 Next we consider the regime where the jet splits dur-
 432 ing the transition seasons. This occurs for long orbital
 433 periods, intermediate obliquity, and intermediate-to-fast
 434 rotation rates. Figure 6 shows the detailed evolution of
 435 the zonal mean zonal wind, mean meridional circula-
 436 tion, temperature and eddy momentum fluxes for this
 437 case. Although the most noticeable split occurs during

438 late winter-spring transition, there is a weaker jet split
 439 during early winter-fall (e.g., see southern hemisphere in
 440 the rightmost column in Fig. 6). Both split jets result
 441 from similar dynamics that relate to the seasonal cycle
 442 of the Hadley circulation. In the transition seasons, the
 443 circulation is close to hemispherically symmetric, and
 444 due to the relatively fast rotation rate, the cells span
 445 only up to midlatitudes ($\sim 30^\circ$, rightmost column in
 446 Fig. 6), and the thermally driven jet is in the descend-
 447 ing edge of the Hadley circulation. The polar latitudes
 448 during early and late winter are colder than the midlati-
 449 tudes, resulting in steep meridional temperature gradi-
 450 ents that maintain the eddy-driven jet there (Fig. 6). In
 451 contrast, during midwinter the Hadley circulation be-
 452 comes cross-equatorial, and its descending edge reaches
 453 higher latitudes (two left columns in Fig. 6). This re-
 454 sults in a poleward shift of the thermally driven jet and
 455 merging of the thermally driven jet with the eddy driven
 456 jet (Fig. 6). The split of the jet into its thermally- and
 457 eddy-driven components also occurs on Earth (Lachmy
 458 & Harnik 2014; Yuval et al. 2018), however, it is local-
 459 ized and less robust. In addition, a split jet was found
 460 in previous modeling studies of planets with a seasonal
 461 cycle due to non-zero eccentricity, where they were also
 462 related to long orbital periods (Guendelman & Kaspi
 463 2020). This points to a characteristic eddy timescale
 464 that allows this phenomenon to develop mainly for long
 465 enough orbital periods.

3.5. Double jet with varying seasonality

466
 467 At high obliquities and intermediate-slow rotation
 468 rates the seasonality of the westerly jets are very com-
 469 plex (Fig. 2D). For the case shown in Fig. 3 the jet weak-
 470 ens during midwinter and splits during the transitions
 471 seasons. At first glance, this is simply a combination of
 472 the previous two regimes discussed above, the winter jet
 473 weakening and the late winter jet splitting. However, a
 474 deeper examination shows substantial differences in the
 475 vertical temperature structure and dynamics. Different
 476 than the low obliquity case, where the polar latitudes
 477 in the upper atmosphere are colder than the midlati-
 478 tudes, in the high obliquity case they are warmer. This
 479 leads to both a temperature inversion in the vertical
 480 and a reversed meridional temperature gradient at the
 481 top of the atmosphere (Fig. 7). This temperature struc-
 482 ture and the fast radiative transitions that occur at high
 483 obliquities results in the complex seasonal cycle seen in
 484 high obliquities and intermediate rotation rates.

485 During autumn-early winter, there are two different
 486 jets in the winter hemisphere, one jet at the descending
 487 edge of the Hadley circulation and a weaker polar jet
 488 that results from the temperature gradients in the po-

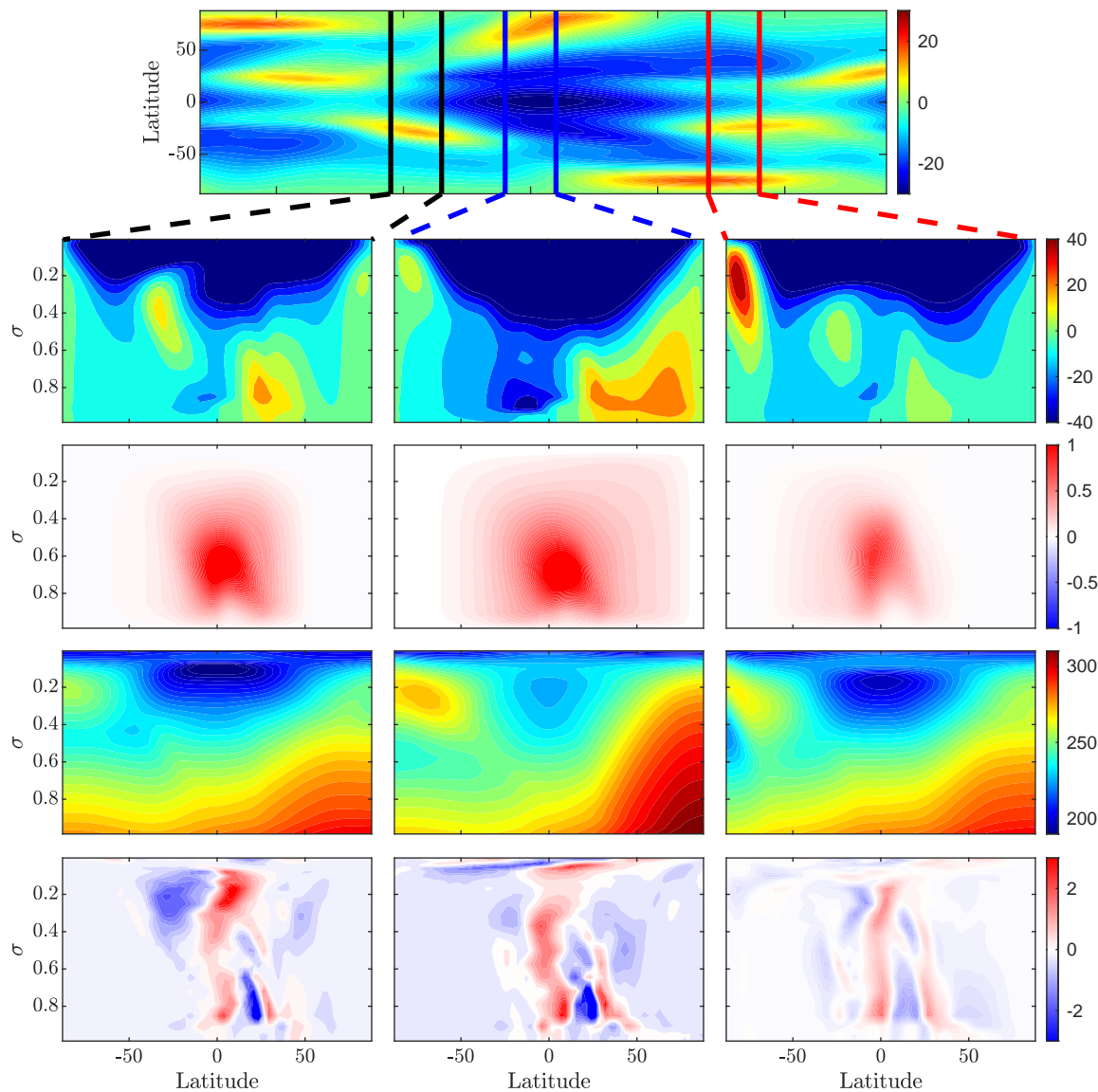


Figure 7. Top row: The zonal mean zonal wind (ms^{-1}) southern hemisphere seasonal cycle around southern hemisphere winter for $\omega = 1$, $\gamma = 70^\circ$ and $\Omega = 0.5$. Vertical lines represent the time average period for the respective column shown below. Second row: The zonal mean zonal wind (ms^{-1}). Third row: mean meridional circulation (Kg s^{-1}). Fourth row: The vertical structure of temperature (K). Fifth row: Eddy momentum flux convergence (ms^{-2}).

lar latitudes. During midwinter, the Hadley circulation widens, and the jets merge. Similar to the midwinter jet weakening regime discussed previously, the widening of the Hadley circulation results in weaker temperature gradients and a weaker jet (Fig. 7). In late winter and the beginning of spring, the Hadley circulation narrows, a jet forms in the descending region of the winter cell and separates from the polar jet that strengthens due to the cooling of the mid-troposphere. As a result of the complexity of the seasonal cycle and the response of the meridional circulation, the subtropical jet is centered

in the mid-troposphere inside the Hadley cell (Fig. 7, around latitude 30° and $\sigma = 0.5$), rather than the edge of the circulation. In addition, there is only weak eddy momentum flux convergence in all the jets, suggesting that the jets are mainly thermally driven.

In addition to the winter jets, in this case, we can see the dominance of the summer jet (middle panel in Fig. 7). This summer jet is discussed in detail in Guendelman et al. (2021), and is related to the widening of Hadley circulation and the increased efficiency of verti-

cal momentum transport with decreasing rotation rate at high obliquity.

Finally, we note that in this regime, the complex seasonal cycle at high obliquities results from the temperature response to the radiative forcing. This could be the result of the simplified radiation scheme used in this model. However, Kang (2019) using a different model showed a similar vertical temperature structure, with warmer poles at higher levels, for high obliquity. This indicates that this is not a model issue, and is a robust response to the high obliquity radiative forcing.

4. RELATION BETWEEN THE JET AND STORM ACTIVITY

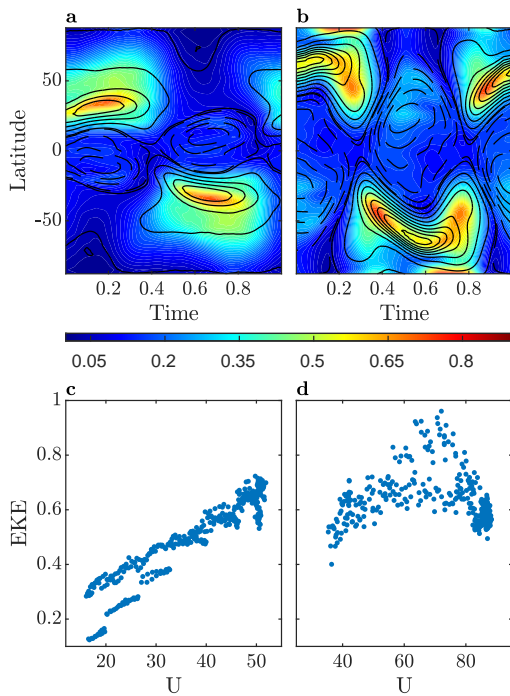


Figure 8. Top: Vertically integrated EKE (shading, 10^6 Jm^{-2} , Eq. 1) and zonal mean zonal wind (contours, contour intervals are 10 ms^{-1}) seasonal cycle at a height of $\sigma = 0.3$ for an Earth-like simulation (a) and for a simulation with $\omega = 4$, $\gamma = 30^\circ$ and $\Omega = 1/2$ (b, the same simulation used for the late winter jet split). Bottom, scatter plot of vertically integrated EKE (10^6 Jm^{-2}) as a function of the jet strength (ms^{-1}) for an Earth-like simulation (c) and for a simulation with $\omega = 4$, $\gamma = 30^\circ$ and $\Omega = 1/2$ (d). Each point represents the value of vertically integrated EKE for the maximum latitudinal wind in each given day.

The jet regions are usually collocated with a region of increased storm activity, a result of the increased baroclinicity in the jet region (Vallis 2017). The storm activity is measured here as the variance of the total kinetic energy, expressed as the vertically integrated eddy ki-

netic energy (EKE)

$$[\text{EKE}] = \int \frac{u'^2 + v'^2}{2} \frac{dp}{g}, \quad (1)$$

where u' and v' are the deviations from the zonal mean (\bar{u}, \bar{v}) and square brackets denote vertical integration. Linear baroclinic instability theory predicts that EKE will increase with increasing jet strength (Charney 1947; Eady 1949). However, this is not the case in all our simulations, and in some cases the EKE is weaker during periods when the jet is strongest. The occurrence of this phenomenon is dispersed throughout the parameter space, occurring mainly in intermediate obliquity values with either long orbital period or intermediate rotation rates. For simplicity, we use the example simulation of the late-winter jet split regime ($\Omega = 1/2$, $\gamma = 30^\circ$ and $\omega = 4$) also as an example of an - EKE minimum simulation. However, suppression of storm activity and late-winter jet split do not always occur together.

In both the Earth-like and EKE minimum simulations, the jet reaches its maximum strength during mid-winter (Fig. 3 and 8a-b). However, the response of the EKE is different between the two. In the Earth-like simulation, the EKE follows the strengthening of the jet. In the EKE minimum simulation, the EKE maximizes during the transition seasons and is weaker during mid-winter. Focusing on the EKE minimum scenario, during autumn-early winter, the jet is in the descending edge of the Hadley cell and can be characterized as a merged jet, where the poleward flank of the jet is eddy driven, which is evident from both the Ferrel cell close to the winter pole and the eddy momentum flux convergence there (Fig. 6). During midwinter, with the widening of the Hadley cell, the jet shifts poleward and strengthens. The eddy momentum flux convergence is weaker compared to the transition seasons (Fig. 6), as well as the EKE (Fig. 8b). During late winter, the jet shifts equatorward and splits into a merged jet and an eddy-driven jet (Fig. 6 and 8), and EKE starts to strengthen again.

A similar minimum of EKE occurs on Earth over the Pacific (Nakamura 1992); however, there are different characteristics between the two. First, on Earth, the jet shifts equatorward during midwinter, unlike our simulation, where it shifts poleward. In addition, the jet on Earth transitions from a merged jet during the transition season to a more subtropical, thermally driven jet during midwinter (e.g., Yuval et al. 2018). While there are these differences in characteristics, the explanation for the EKE minimum on Earth proposed by Hadas & Kaspi (2021) who connected the decrease in EKE with a decrease in the number of storms and the storms lifetime due to a disconnect between the upper

578 and lower levels with the increasing jet strength can also
 579 apply for our simulations, given the similar jet speed
 580 dependence. When comparing the Earth-like and EKE
 581 minimum simulations, at lower jet speeds we can see a
 582 similar jet strength dependence (Fig. 8c-d). However,
 583 the jet in the EKE minimum simulation reaches higher
 584 speeds than in the Earth-like simulation, and surpasses a
 585 threshold where EKE starts to decrease with increasing
 586 jet strength (Fig. 8c-d). This holds more generally, with
 587 mid-winter minimum in EKE occurring in simulations
 588 where the jet speed exceeds around 60-70 m/s. In addition,
 589 as the jet strengthens, it also narrows (Fig. 8b),
 590 and Harnik & Chang (2004) have shown that as the jet
 591 narrows there is a decrease in the meridional wavelength
 592 of the perturbation resulting in the perturbations growing
 593 less, and this can be an explanation of the EKE
 594 minimum.

595 5. POTENTIAL VORTICITY STRUCTURE

596 The potential vorticity (PV) is a useful quantity when
 597 studying the dynamics of vortices (Hoskins et al. 1985),
 598 as in the absence of diabatic forcing and friction PV acts
 599 as a conserved tracer. We calculate the PV using

$$600 \quad PV = g(f + \zeta) \frac{\partial \theta}{\partial p}, \quad (2)$$

601 where g is the surface gravity, $f = 2\Omega \sin \phi$, ϕ is latitude,
 602 θ is the potential temperature, and ζ is the vertical com-
 603 ponent of the relative vorticity given by

$$604 \quad \zeta = \frac{1}{a \cos \phi} \frac{\partial v}{\partial \lambda} - \frac{1}{a \cos \phi} \frac{\partial}{\partial \phi} (u \cos \phi), \quad (3)$$

605 where λ is longitude. Because PV can vary signifi-
 606 cantly in its vertical structure, we follow previous studies
 607 (e.g., Lait 1994; Mitchell et al. 2015; Waugh et al. 2016;
 608 Sharkey et al. 2021) and use the scaled PV given by

$$609 \quad PV_s = PV \left(\frac{\theta}{\theta_0} \right)^{-(1+R/c_p)}, \quad (4)$$

610 where θ_0 is a reference potential temperature. This form
 611 removes a significant amount of the PV vertical varia-
 612 tion.

613 In Earth's atmosphere, PV generally monotonically
 614 increases (in absolute values) from the equator to the
 615 poles. However, this is not the case on Mars (e.g.,
 616 Mitchell et al. 2015) or Titan (Sharkey et al. 2020, 2021),
 617 where the PV has an annular structure, i.e., it maximizes
 618 equatorward from the poles. The persistence of an annu-
 619 lar PV structure is somewhat surprising as past studies
 620 have shown that an annular PV structure is barotrop-
 621 ically unstable (Dritschel & Polvani 1992). Given this,

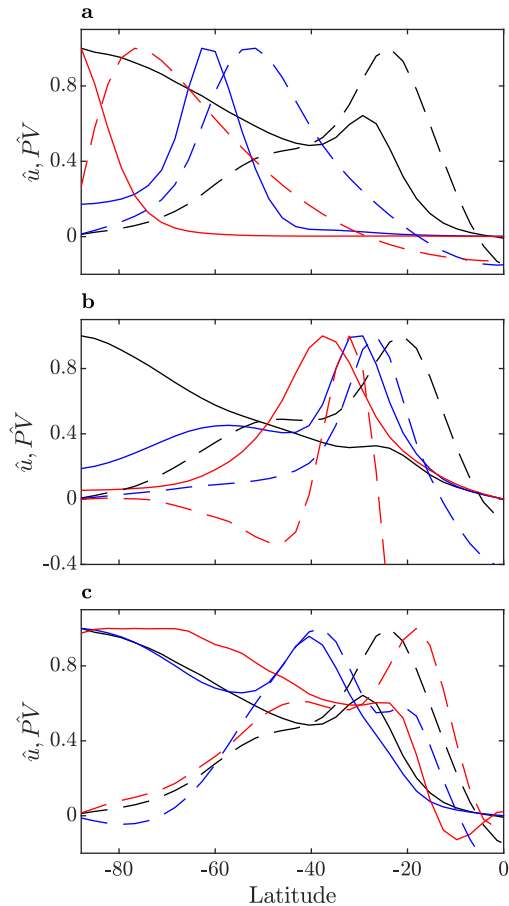


Figure 9. PV (solid) and zonal mean zonal wind (dashed) meridional structure in the winter hemisphere, for different parameter values for a temporal mean of days 180-240 and $\sigma = 0.5$. Each line is normalized by its maximum value. (a) black is for $\Omega = 1$, blue is for $\Omega = 1/4$ and red is for $\Omega = 1/16$, other parameters are constant with $\omega = 1$ and $\gamma = 30^\circ$. (b) black is for $\gamma = 20^\circ$, blue is for $\gamma = 50^\circ$ and red is for $\gamma = 80^\circ$, other parameters are constant with $\omega = 1$ and $\Omega = 1$. (c) black is for $\omega = 1$, blue is for $\omega = 4$ and red is for $\omega = 4$, other parameters are constant with $\Omega = 1$ and $\gamma = 30^\circ$.

622 studies of the Martian polar vortex have suggested that
 623 forcing is needed to maintain the annular structure (e.g.,
 624 Mitchell et al. 2015). Toigo et al. (2017) suggested that
 625 latent heating from CO_2 condensation is what forces
 626 the annular PV structure on Mars. In addition to that,
 627 Scott et al. (2020) have shown, using a simplified shallow
 628 water model, that annular PV can also be maintained
 629 solely due to transport from the Hadley circulation.

630 To examine the dependence of the PV structure on the
 631 different planetary parameters, it is insightful to com-
 632 pare the latitudinal structures of PV together with that
 633 of the zonal mean zonal wind. For a close to Earth-like
 634 configuration (black lines in Fig. 9a), the jet is at around
 635 20° and the strongest PV meridional gradients occur

636 close to this latitude. There is a local maximum in the
 637 PV near the jet, but it is not a global maximum, and the
 638 PV maximizes at the pole (black lines in Fig. 9a). De-
 639 creasing the rotation rate results in two main responses:
 640 the jet shifts poleward, and the background vorticity
 641 (i.e., the Coriolis parameter f) weakens. The combina-
 642 tion of these changes results in a global maximum of PV
 643 poleward of the jet, with the maximum PV gradient is
 644 still close to the maximum winds. In intermediate rota-
 645 tion rates, where the jet is not too close to the pole, this
 646 results in an annular PV (e.g., $\Omega = 1/4$, blue curves in
 647 Fig. 9a). For slow rotation the jet is close to the pole
 648 and maximum PV is at the pole (e.g., $\Omega = 1/16$, red
 649 curves in Fig. 9a).

650 Increasing the obliquity shifts the jet poleward and
 651 and makes it narrower (black to blue to red dashed
 652 curves in Fig. 9b). This, in turn, increases the effect
 653 of relative vorticity, allowing, in some cases for an annu-
 654 lar PV to persist (Fig. 9b). Increasing the orbital period
 655 also results in a shift poleward of the vortex; however,
 656 the narrowing effect seen with increasing obliquity is less
 657 dominant (Fig. 9c).

658 There is a trade-off between increasing obliquity and
 659 decreasing rotation rate when considering the polar vor-
 660 tex PV structure. For fast rotation rates, cases with
 661 high obliquity have annular PV (Fig. 9b), and as the ro-
 662 tation rate decreases, it shifts to a monopolar PV, as the
 663 polar vortex is closer to the pole (Fig. 9a). An opposite
 664 effect occurs at low obliquity values. For fast rotation
 665 rates, the PV is monopolar, while for the same obliqu-
 666 ity value, an annular PV can persist in slower rotation
 667 rates, up to the point where the vortex reaches close to
 668 the pole (Fig. 11)

669 The above analysis focused on the winter polar vor-
 670 tex. However, for slow rotation rates and high obliquity
 671 the dominant jet is in the summer hemisphere (Guen-
 672 delman et al. 2021). The PV structure of the summer
 673 hemisphere polar vortex for different values of obliquity
 674 are shown in Fig. 10. For low obliquity, the low-level
 675 jet is not fully developed, and the dominant jet in the
 676 summer hemisphere is the subtropical jet. Due to the
 677 slow rotation, the PV has an annular structure (black
 678 lines in Fig. 10), similar to the winter polar vortex in
 679 intermediate rotation rates. For higher obliquities (blue
 680 and red lines in Fig. 10) the low-level summer jet dom-
 681 inates, and there is a step-like structure, where PV in
 682 the poleward flank of the vortex is constant with steep
 683 PV gradients equatorward and poleward of it.

684 The PV characteristics changes not only with the
 685 planetary parameters but also during the seasonal cycle,
 686 and the PV can shift between monopolar and annular
 687 during the year. Fig 11 shows the seasonal cycle of PV

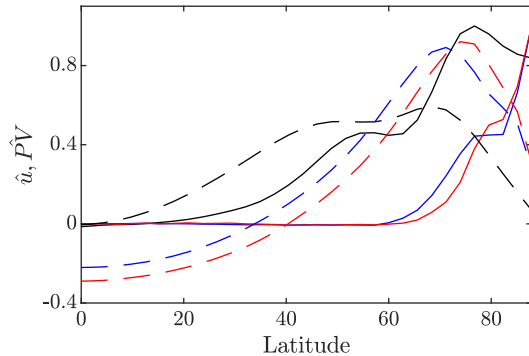


Figure 10. PV (solid) and zonal mean zonal wind (dashed) meridional structure in the summer hemisphere for different parameter values for a temporal mean of days 180-240 and vertically averaged between $\sigma = 0.5$ and $\sigma = 0.85$. Each line is normalized by its maximum value in the summer hemisphere. Black is for $\gamma = 20^\circ$, blue is for $\gamma = 50^\circ$ and red is for $\gamma = 80^\circ$, other parameters are constant with $\omega = 1$ and $\Omega = 1/16$.

688 (shading) and zonal mean zonal wind for different val-
 689 ues of rotation rate with $\gamma = 30^\circ$ and $\omega = 1$. At fast
 690 rotation rate ($\Omega = 1$, top panel in Fig. 11), similar to
 691 the seasonal mean, in the jet vicinity there is a local
 692 PV maximum, however the global maximum is at the
 693 pole. At lower rotation rates, there are cases where the
 694 polar vortex has an annular PV during the entire winter
 695 ($\Omega = 1/2$ second panel in Fig. 11). However, for
 696 slow rotation rates ($\Omega \leq 1/4$, bottom three panels in
 697 Fig. 11) the polar vortex PV shifts between annular and
 698 monopolar.

699 To get a better intuition for why there exists an an-
 700 nular PV in some parts of the parameter space, it is in-
 701 sightful to consider the case where $\partial_p \theta$ is approximately
 702 constant. The main variations in the zonal-mean PV
 703 are then due to the competing effects of the planetary
 704 vorticity, i.e., the Coriolis term $f = 2\Omega \sin \phi$ and the
 705 zonal-mean relative vorticity $\bar{\zeta} = \frac{1}{a \cos \phi} \frac{\partial}{\partial \phi} (\bar{u} \cos \phi)$. The
 706 rotation rate is the only parameter that contributes to
 707 changes in the background planetary vorticity, but all
 708 the parameters can cause changes in meridional struc-
 709 ture of the zonal wind (and hence the relative vorticity).
 710 Changes in the zonal wind can be expressed as changes
 711 in the latitude, strength, and width of the jet, and to
 712 better understand the role of these jet characteristics on
 713 the PV structure, we assume a Gaussian jet of the form

$$714 \quad U = U_0 \exp \left[-\frac{(\phi + \phi_0)^2}{2\phi_w^2} \right]. \quad (5)$$

715 This corresponds to a jet centered around latitude $-\phi_0$
 716 with a characteristic width of ϕ_w and a strength of U_0 .
 717 The effect of independent changes in the jet strength,

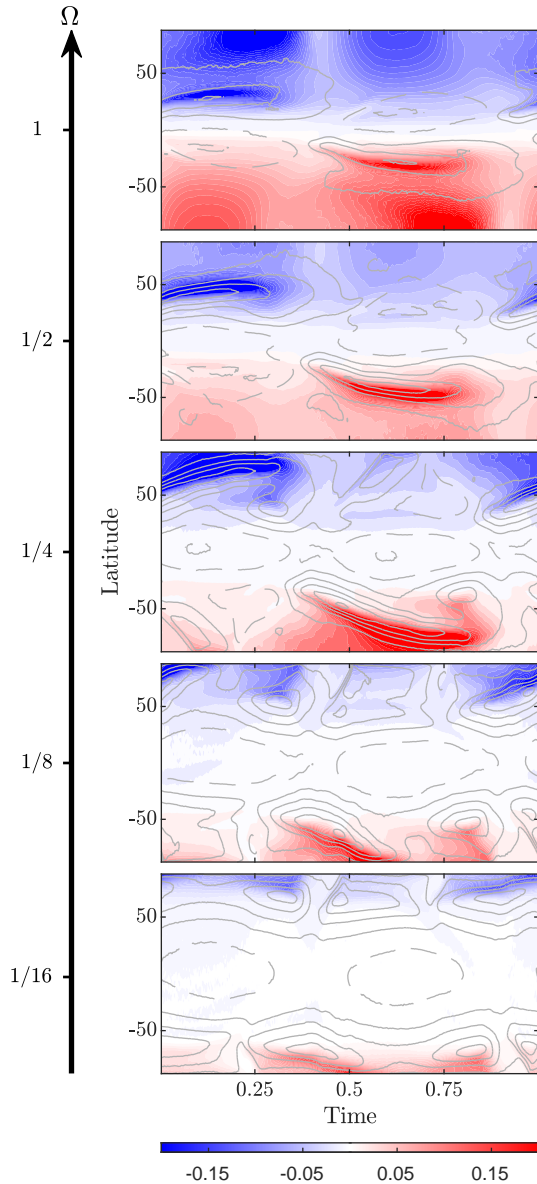


Figure 11. The potential vorticity (shading, $10^{-6} \text{ Km}^2\text{s}^{-1}\text{Kg}^{-1}$) and zonal mean zonal wind (contours, contour interval 10ms^{-1}) seasonal cycle at a height of $\sigma = 0.5$ for different values of rotation rates (Ω) with $\gamma = 30^\circ$ and $\omega = 1$.

latitude, and width, as well as rotation rate are shown in Fig. 12. The rotation rate has the most significant effect on the PV structure, with annular vortex occurring as rotation rate decreases. The changes in jet characteristics have a comparable impact on the meridional structure of the PV near the jet, but whether this causes an annular structure (higher or lower values at the pole than at the jet) differs between characteristics. Changing the strength or width of the jet changes the PV gradients at jet, and can lead to a local maximum, but

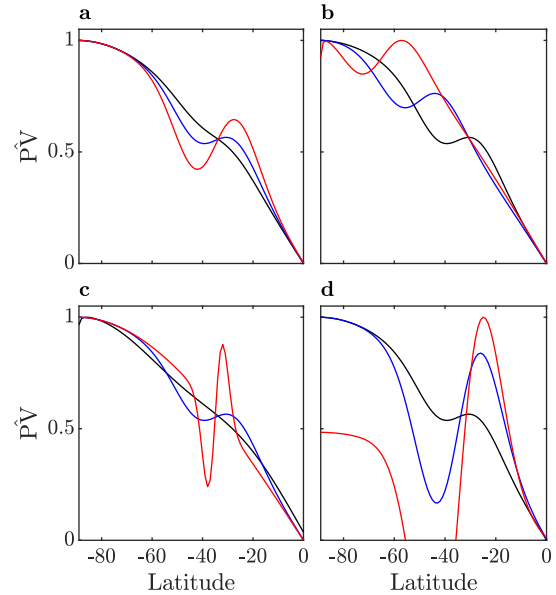


Figure 12. The value of $f + \bar{\zeta}$ normalized (each line is normalized by its maximum) using Eq. 5 for the zonal mean zonal wind for different vortex strengths (a, $U_0 = 10$, black, $U_0 = 30$, blue, $U_0 = 60$, red), Vortex latitude (b, $\phi_0 = 35^\circ$, black, $\phi_0 = 50^\circ$, blue, $\phi_0 = 65^\circ$, red), Vortex width (c, $\phi_w = 20^\circ$, black, $\phi_w = 10^\circ$, blue, $\phi_w = 3^\circ$, red) and rotation rates (d, $\Omega = 1$, black, $\Omega = 1/4$, blue, $\Omega = 1/16$, red). Default parameter values are $U_0 = 30$, $\phi_0 = 35^\circ$, $\phi_w = 10^\circ$, $\Omega = 1$.

not an annular vortex (for jets centered around 35°) (Fig. 12a,c). However, moving the jet towards the pole can form an annular structure, especially when the jet is at high latitudes, but not too close to the pole (Fig. 12b). This is a result of the weak planetary vorticity gradients at high latitudes, which means a relatively small effect from ζ can result in an annular structure. Note that this analysis is highly simplified, but can provide insight into the effect of the different planetary parameters on the PV structure. For example, decreasing the rotation rate not only decreases the planetary vorticity, but also causes a poleward shift of the jet (Fig. 9a), both contributing to the annular PV in the intermediate rotation rates (for slow rotation the jet is too close to the pole in slow rotation rates, resulting in a monopolar PV). Alternatively, as the obliquity increases, the vortex goes more poleward and becomes narrower, which results in annular PV for high obliquity and fast rotation rate (Fig. 9).

6. CONCLUSIONS

We have examined the dependence of the structure and seasonal characteristics of polar vortices in terrestrial planets on obliquity, orbital period, and rotation rate. For parameters close to Earth, the simulated vortex structure and evolution is similar to the observed on

Earth (Fig. 3). However, away from Earth’s parameters we find a wide range in the vortex characteristics and seasonality. Specifically, in addition to the Earth-like regime, we identify the following regimes:

1. Weak seasonality, normal climate: The jet is in the low- and mid-latitudes with weak seasonality. This regime occurs in obliquities lower than $\sim 54^\circ$ and short orbital periods ($\omega \leq 1/8$).
2. Weak seasonality, reversed climate: The temperature latitudinal profile in these cases is reversed, with maximum temperature at the poles and minimum at the equator. The flow is dominated by a wide equatorial westerly jet, with essentially no polar vortex (Fig. 4). This regime occurs in obliquities higher than $\sim 54^\circ$ and short orbital periods ($\omega \leq 1/8$).
3. Winter jet weakening: The jet experiences a weakening during midwinter. This weakening results from the winter Hadley circulation spanning from one pole to the other with air descending close to the winter pole and warming these regions adiabatically. As a result, the meridional temperature gradients are flat during midwinter, and the jet weakens. This regime occurs for slow rotation rates with high enough obliquity ($\gamma \geq 30^\circ$, depending on the rotation rate and orbital period).
4. Late winter jet split: The polar jet splits during late winter and spring as the Hadley circulation contracts, and becomes more hemispherically symmetric. The jet shifts equatorward and splits into its thermally- and eddy- driven components, with the thermally-driven jet located at the edge of the Hadley circulation. This regime occurs for cases with long enough orbital period.
5. Double jet with varied seasonality: The zonal mean zonal wind exhibits a complex seasonal cycle with periods of a double jet and a merged jet, together with a jet weakening during midwinter. In this cases, the temperature structure at the top of the atmosphere is reversed with the warmest high-level temperatures at the pole. As a result, in addition to the jet at the edge of the Hadley cell, there is a thermally driven jet that is disconnected from the Hadley circulation during the transition seasons. During winter, as the Hadley circulation expand to higher latitudes the jets merge. Additionally, due to the high latitude being warm in high levels, meridional temperature gradients are

flat, and there is a weakening of the polar vortex during midwinter. This regime occurs at high obliquities and intermediate-slow rotation rates.

Although our model is idealized, our results are not detached from the natural world as similar behaviors seen in our simulations are observed in the solar system terrestrial planets. In addition to the Earth-like regime which corresponds also to the polar vortex seasonal cycle on Mars (e.g., [Vaugh et al. 2016](#)), the winter jet weakening regime has some similarities to the seasonal cycle of Titan’s polar vortex. There are increasing evidence that Titan’s polar vortex exhibits sudden warming during midwinter ([Teanby et al. 2019](#)). Additionally, Titan atmospheric models also show a midwinter polar vortex weakening ([Lora et al. 2015](#)). Both the model results and the observed warming of the vortex align well with our simulations. At slow rotation rates, during midwinter, the circulation expands, and there is a warming of polar latitudes resulting from air descending there. This polar warming and the wide Hadley circulation flattens the meridional temperature gradient resulting in a weaker vortex during midwinter.

We have also found other distinct polar vortex behaviors, that have no counterpart in our solar system. Some of this, such as the normal and reverse weak seasonality regimes were previously studied in studies that neglected the seasonal cycle (e.g., [Kaspi & Showman 2015](#); [Kang et al. 2019](#)), and can be relevant for planets with a massive atmosphere, cold planets (high atmospheric radiative timescale), or ocean worlds (high surface thermal inertia) such that they experience a weak seasonal cycle. Others, such as the double jet regime, were not previously studied. A feature unique to the double jet regime is the vertical temperature structure close to the pole, where at high obliquities, there is a strong reversal of temperature gradients with maximum temperature at the pole in high levels. Given the simplified radiation scheme used in this model, there is a need to explore the sensitivity of the temperature response to different radiative parameters such as the long- and short-wave optical depths and how it is sensitive to different radiation schemes.

In addition, we have also shown that the potential vorticity (PV) meridional structure of the polar vortices can be very different from Earth’s polar vortices. On Earth, the maximum PV is at the vortex center, but we have shown that annular PV is not uncommon within the planetary parameter space explored. Across the parameter space there is high (absolute) PV poleward of the jet, with large meridional PV gradients at the jet. However, the details vary with the parameters. In particular, the gradients of PV within the vortex vary,

with cases with a monotonic increase in PV towards the pole (monopolar vortex, similar to Earth's polar vortex), global PV maximum around the peak winds and a decrease towards the pole (annular vortex, similar to Mars's and Titan's polar vortex), or a local maximum of PV close to the jet and a global maximum at the pole. These variations depend on the planetary potential vorticity (i.e., rotation rate) and the vortex characteristics, mainly the vortex latitude, width, and strength that depend on the different planetary parameters. It is important to note that similarly to Scott et al. (2020), the maintenance of an annular PV in these simulations is mainly a result of Hadley circulation transport. This suggests that although on Mars, where there is a need for latent forcing to maintain an annular PV (Seviour et al. 2017), this is not needed in general.

We have also shown the appearance of storm activity suppression during midwinter, when the jet is the strongest. This suppression of storms during midwinter is also observed on Earth (e.g., Nakamura 1992; Afargan & Kaspi 2017) and on Mars (e.g., Lewis et al. 2016). However, the suppression of storm activity on Earth, Mars and our simulations shows different characteristics one from another. For example, on Earth the jet becomes more thermally driven and shift equatorward during midwinter (e.g., Yuval et al. 2018), which does not occur in our simulations. Unlike Earth and our simulations, the suppression of baroclinic activity on Mars is confined to lower levels close to the surface (e.g., Lewis et al. 2016). Yet, the existence of midwinter minimum

in our simulations aligns with other explanations such as the jet narrowing as it strengthens (Harnik & Chang 2004) or a threshold in the jet strength (Hadas & Kaspi 2021). The differences in characteristics between the planets and with our simulations need further study to explore how planetary parameters and atmospheric characteristics affect the relation between storms and the polar vortex.

The fact that the polar vortices in our idealized model have jet strength, seasonality and PV structure comparable to the observed polar vortices on terrestrial planets suggest that the dynamics observed on the solar system terrestrial planets relate to basic dynamical processes that occur in planetary atmospheres rather than specific processes that occur in a specific planet's atmosphere. This, in turn, suggest that on planets outside of the solar system, there will be a large variety of climates that can also vary significantly during the seasonal cycle depending on the planetary parameters. This can also substantially impact future observations from planets, and future studies need to account for this variability.

IG and YK acknowledge support from the Minerva Foundation and the Helen Kimmel Center of Planetary Science at the Weizmann Institute of Science. DW acknowledges support from the U.S. National Science Foundation and National Aeronautics and Space Administration.

REFERENCES

- Adriani, A., Mura, A., Orton, G., et al. 2018, *Nature*, 555, 216, doi: [10.1038/nature25491](https://doi.org/10.1038/nature25491)
- Afargan, H., & Kaspi, Y. 2017, *Geophysical Research Letters*, 44, doi: [10.1002/2017GL075136](https://doi.org/10.1002/2017GL075136)
- Charney, J. G. 1947, *Journal of Atmospheric Sciences*, 4, 136, doi: [10.1175/1520-0469\(1947\)004<0136:TDOLWI>2.0.CO;2](https://doi.org/10.1175/1520-0469(1947)004<0136:TDOLWI>2.0.CO;2)
- Dritschel, D. G., & Polvani, L. M. 1992, *Journal of Fluid Mechanics*, 234, 47, doi: [10.1017/S0022112092000697](https://doi.org/10.1017/S0022112092000697)
- Dyudina, U. A., Ingersoll, A. P., Ewald, S. P., et al. 2008, *Science*, 319, 1801, doi: [10.1126/science.1153633](https://doi.org/10.1126/science.1153633)
- Eady, E. T. 1949, *Tellus*, 1, 33
- French, R. G., & Gierasch, P. J. 1979, *Journal of Geophysical Research*, 84, 4634, doi: [10.1029/JB084iB09p04634](https://doi.org/10.1029/JB084iB09p04634)
- Frierson, D. M. W., Held, I. M., & Zurita-Gotor, P. 2006, *Journal of the Atmospheric Sciences*, 63, 2548, doi: [10.1175/JAS3753.1](https://doi.org/10.1175/JAS3753.1)
- Guendelman, I., & Kaspi, Y. 2018, *Geophysical Research Letters*, 45, doi: [10.1029/2018GL080752](https://doi.org/10.1029/2018GL080752)
- . 2019, *The Astrophysical Journal*, 881, 67, doi: [10.3847/1538-4357/ab2a06](https://doi.org/10.3847/1538-4357/ab2a06)
- . 2020, *The Astrophysical Journal*, 901, 46. <https://iopscience.iop.org/article/10.3847/1538-4357/abaef8>
- Guendelman, I., Waugh, D. W., & Kaspi, Y. 2021, *Journal of the Atmospheric Sciences*, 78, 3337, doi: [10.1175/JAS-D-21-0019.1](https://doi.org/10.1175/JAS-D-21-0019.1)
- Hadas, O., & Kaspi, Y. 2021, *Journal of the Atmospheric Sciences*, 78, 2445, doi: [10.1175/JAS-D-20-0289.1](https://doi.org/10.1175/JAS-D-20-0289.1)
- Harnik, N., & Chang, E. K. M. 2004, *Journal of the Atmospheric Sciences*, 61, 23, doi: [10.1175/1520-0469\(2004\)061<0023:TEOVIJ>2.0.CO;2](https://doi.org/10.1175/1520-0469(2004)061<0023:TEOVIJ>2.0.CO;2)
- Hoskins, B. J., McIntyre, M. E., & Robertson, A. W. 1985, *Quarterly Journal of the Royal Meteorological Society*, 111, 877, doi: <https://doi.org/10.1002/qj.49711147002>

- 944 Kang, W. 2019, *The Astrophysical Journal*, 877, L6,
945 doi: [10.3847/2041-8213/ab1f79](https://doi.org/10.3847/2041-8213/ab1f79)
- 946 Kang, W., Cai, M., & Tziperman, E. 2019, *Icarus*, 330, 142,
947 doi: <https://doi.org/10.1016/j.icarus.2019.04.028>
- 948 Kaspi, Y., & Showman, A. P. 2015, *The Astrophysical*
949 *Journal*, 804, 60, doi: [10.1088/0004-637X/804/1/60](https://doi.org/10.1088/0004-637X/804/1/60)
- 950 Lachmy, O., & Harnik, N. 2014, *jas*, 71, 1389,
951 doi: [10.1175/JAS-D-13-0125.1](https://doi.org/10.1175/JAS-D-13-0125.1)
- 952 Lait, L. R. 1994, *Journal of Atmospheric Sciences*, 51, 1754
953 , doi: [10.1175/1520-0469\(1994\)051\(1754:
954 AAFFPV\)2.0.CO;2](https://doi.org/10.1175/1520-0469(1994)051(1754:AAFFPV)2.0.CO;2)
- 955 Lee, C., Richardson, M. I., Newman, C. E., & Mischna,
956 M. A. 2018, *Icarus*, 311, 23,
957 doi: <https://doi.org/10.1016/j.icarus.2018.03.019>
- 958 Lewis, S. R., Mulholland, D. P., Read, P. L., et al. 2016,
959 *Icarus*, 264, 456,
960 doi: <https://doi.org/10.1016/j.icarus.2015.08.039>
- 961 Lora, J. M., Lunine, J. I., & Russell, J. L. 2015, *Icarus*, 250,
962 516, doi: [10.1016/j.icarus.2014.12.030](https://doi.org/10.1016/j.icarus.2014.12.030)
- 963 Luz, D., Berry, D. L., Piccioni, G., et al. 2011, *Science*, 332,
964 577, doi: [10.1126/science.1201629](https://doi.org/10.1126/science.1201629)
- 965 Mitchell, D. M., Montabone, L., Thomson, S., & Read,
966 P. L. 2015, *Quarterly Journal of the Royal Meteorological*
967 *Society*, 141, 550, doi: [10.1002/qj.2376](https://doi.org/10.1002/qj.2376)
- 968 Mulholland, D. P., Lewis, S. R., Read, P. L., Madeleine,
969 J.-B., & Forget, F. 2016, *Icarus*, 264, 465,
970 doi: <https://doi.org/10.1016/j.icarus.2015.08.038>
- 971 Nakamura, H. 1992, *Journal of the Atmospheric Sciences*,
972 49, 1629, doi: [10.1175/1520-0469\(1992\)049\(1629:
973 MSOBWA\)2.0.CO;2](https://doi.org/10.1175/1520-0469(1992)049(1629:MSOBWA)2.0.CO;2)
- 974 Polvani, L. M., Sobel, A. H., & Waugh, D. W., eds. 2010,
975 *Geophysical Monograph Series*, Vol. 190, *The*
976 *Stratosphere: Dynamics, Transport, and Chemistry*
977 (Washington, D. C.: American Geophysical Union),
978 doi: [10.1029/GM190](https://doi.org/10.1029/GM190)
- 979 Scott, R. K., Seviour, W. J. M., & Waugh, D. W. 2020,
980 *Quarterly Journal of the Royal Meteorological Society*,
981 146, 2174, doi: [10.1002/qj.3786](https://doi.org/10.1002/qj.3786)
- 982 Seviour, W. J. M., Waugh, D. W., & Scott, R. K. 2017,
983 *Journal of the Atmospheric Sciences*, 74, 1533,
984 doi: [10.1175/JAS-D-16-0293.1](https://doi.org/10.1175/JAS-D-16-0293.1)
- 985 Sharkey, J., Teanby, N. A., Sylvestre, M., et al. 2020,
986 *Icarus*, 337, 113441, doi: [10.1016/j.icarus.2019.113441](https://doi.org/10.1016/j.icarus.2019.113441)
- 987 —. 2021, *Icarus*, 354, 114030,
988 doi: [10.1016/j.icarus.2020.114030](https://doi.org/10.1016/j.icarus.2020.114030)
- 989 Tan, Z., Lachmy, O., & Shaw, T. A. 2019, *J. Adv. Model.*
990 *Earth Syst.*, 11, 934,
991 doi: <https://doi.org/10.1029/2018MS001492>
- 992 Teanby, N. A., Sylvestre, M., Sharkey, J., et al. 2019,
993 *Geophysical Research Letters*, 46, 3079,
994 doi: [10.1029/2018GL081401](https://doi.org/10.1029/2018GL081401)
- 995 Teanby, N. A., de Kok, R., Irwin, P. G. J., et al. 2008,
996 *Journal of Geophysical Research*, 113, E12003,
997 doi: [10.1029/2008JE003218](https://doi.org/10.1029/2008JE003218)
- 998 Teanby, N. A., Bézard, B., Vinatier, S., et al. 2017, *Nature*
999 *Communications*, 8, 1586,
1000 doi: [10.1038/s41467-017-01839-z](https://doi.org/10.1038/s41467-017-01839-z)
- 1001 Toigo, A. D., Waugh, D. W., & Guzewich, S. D. 2017,
1002 *Geophysical Research Letters*, 44, 71,
1003 doi: [10.1002/2016GL071857](https://doi.org/10.1002/2016GL071857)
- 1004 Vallis, G. K. 2017, *Atmospheric and Oceanic Fluid*
1005 *Dynamics: Fundamentals and Large-Scale Circulation*,
1006 2nd edn. (Cambridge University Press),
1007 doi: [10.1017/9781107588417](https://doi.org/10.1017/9781107588417)
- 1008 Wang, Y., Read, P. L., Tabataba-Vakili, F., & Young, R.
1009 M. B. 2018, *Q. J. R. Meteorol. Soc.*, 144, 2537,
1010 doi: [10.1002/qj.3350](https://doi.org/10.1002/qj.3350)
- 1011 Waugh, D. W., Sobel, A. H., & Polvani, L. M. 2017,
1012 *Bulletin of the American Meteorological Society*, 98, 37,
1013 doi: [10.1175/BAMS-D-15-00212.1](https://doi.org/10.1175/BAMS-D-15-00212.1)
- 1014 Waugh, D. W., Toigo, A. D., Guzewich, S. D., et al. 2016,
1015 *Journal of Geophysical Research: Planets*, 121, 1770,
1016 doi: [10.1002/2016JE005093](https://doi.org/10.1002/2016JE005093)
- 1017 Yuval, J., Afargan, H., & Kaspi, Y. 2018, *Geophysical*
1018 *Research Letters*, 45, 9995, doi: [10.1029/2018GL078678](https://doi.org/10.1029/2018GL078678)